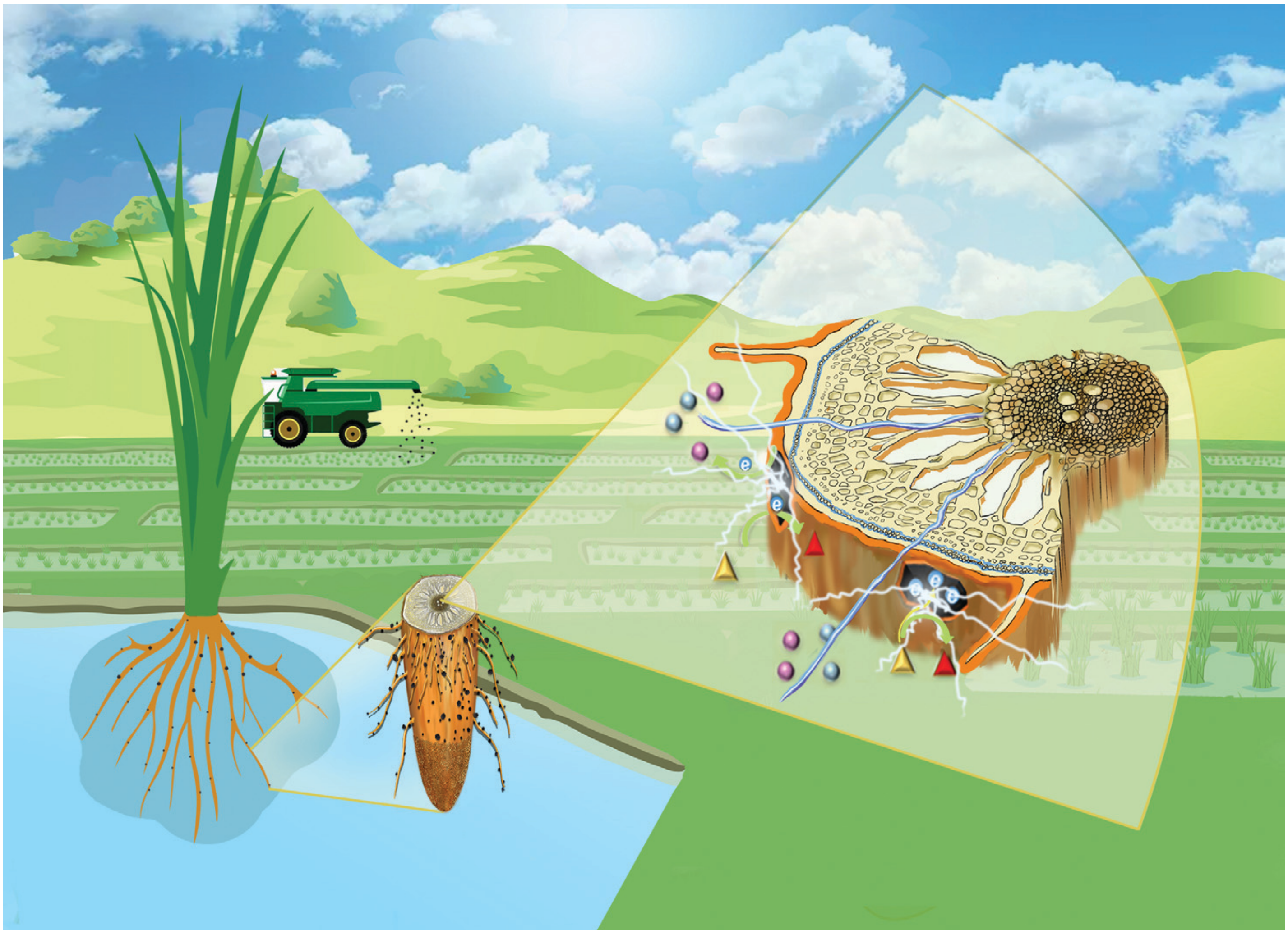

Featuring work from Prof. Fei Lian at School of Energy and Environmental Engineering, Hebei University of Technology, China, and Prof. Zhenyu Wang at Institute of Environmental Processes and Pollution Control, School of Environment and Civil Engineering, Jiangnan University, China.

Nano-biochar modulates the formation of iron plaque through facilitating iron-involved redox reactions on aquatic plant root surfaces

The formation of root iron plaque in aquatic plants can be regulated by the redox properties of attached nano-biochar. Two dominating mechanisms including direct oxidation and electron transfer in the formation of iron plaque induced by nano-BC are recapitulated here.

As featured in:

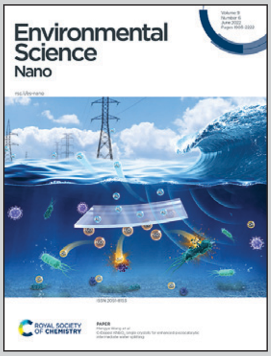
Environmental Science Nano

See Fei Lian, Zhenyu Wang *et al.*, *Environ. Sci.: Nano*, 2022, **9**, 1974.

ROYAL SOCIETY OF CHEMISTRY

rsc.li/es-nano

Environmental
Science
Nano

ROYAL SOCIETY
OF CHEMISTRY

PAPER

View Article Online
View Journal | View Issue

Check for updates

Cite this: *Environ. Sci.: Nano*, 2022, **9**, 1974

Nano-biochar modulates the formation of iron plaque through facilitating iron-involved redox reactions on aquatic plant root surfaces†

Shiguo Gu, [a] Fei Lian, *[b] Yaru Han,[a] Sarasadat Taherymoosavi,[c] David Mitchell,[d] Stephen Joseph,[ce] Zhenyu Wang *[a] and Baoshan Xing [f]

Received 12th January 2022,
Accepted 13th April 2022

DOI: 10.1039/d2en00032f

rsc.li/es-nano

The ubiquitous presence of submicron-sized black carbon (BC) in the water environment makes it inevitably interact with root surfaces of aquatic plants. However, the nexus between catalytic ability of attached BC and iron plaque (IP) formation is not fully understood. Here, the impact of nanoscale BC particles (nano-BC) produced at 400 and 700 °C on Fe(II) oxidation and IP formation (*i.e.*, Fe(III)-(oxyhydr)oxide coating) on root surfaces of rice seedlings was investigated *via* hydroponic culture. Results suggest that the formation of IP was considerably regulated by the concentration of nano-BC attached on roots, where low concentration of nano-BC (10 mg L^{-1} for nano400 and 5 mg L^{-1} for nano700) significantly ($p < 0.05$) enhanced the formation of IP due to Fe(II) direct oxidation/electron transfer while excess nano-BC not only impeded the formation of IP but also significantly reduced ($p < 0.05$) plant growth and nutrient uptake. The critical concentration of nano-BC was highly dependent on its redox potential stemming from both redox-active groups and graphitic structures in nano-BC. The newly formed BC–IP composite exhibited distinct configuration relative to the common IP, where both poorly crystalline Fe(III) (oxyhydr)oxides and Fe-containing nanoparticles were observed. Our findings provide new insights into the nano-BC facilitated formation of IP and its critical role in the growth of aquatic plants.

Environmental significance

Nano-sized black carbon (nano-BC) is ubiquitous in soil and water environments. The high colloidal stability of nano-BC makes it very likely attach to root surfaces of aquatic plants, forming an important root–BC interface to directly affect root reactions with surroundings. The present study demonstrated that the formation and configuration of iron plaque (IP) on rice roots could be regulated by redox properties of attached nano-BC. We observed that Fe(II) direct oxidation and accelerated electron transfer were the dominating mechanisms contributing to the formation of IP from the low- and high-temperature nano-BC, respectively. The newly formed BC–IP composite exhibited a distinct configuration relative to the common IP and thus probably distinct environmental functions, which has profound environmental implications in aquatic systems.

Introduction

Black carbon (BC), the solid pyrolysis products of biomass and fossil fuels, is ubiquitous in the environment and could participate in various biogeochemical processes including sorption for organic compounds and inorganic species,[1] carbon sequestration,[2] and mineral transformation.[3] Although the majority of terrestrial BC (>90%) would remain in the soil environment,[4] a fraction of this pyrogenic material can be released and mobilized into aquatic systems as dissolved BC (DBC), serving as a continuous source of BC to rivers, inland waters, and oceans.[5–7] It was reported that the concentration of DBC ranges from 1.94×10^{-3} to 2.77 mg carbon per L among the freshwater systems.[8] Operationally, the term DBC refers to carbon fractions with diameters less than 0.45 or 0.7 μm,[9,10] which means that DBC is not totally

---

[a] *Institute of Environmental Processes and Pollution Control, and School of Environment and Civil Engineering, Jiangnan University, Wuxi 214122, China. E-mail: wang0628@jiangnan.edu.cn; Tel: +86 0510 85911123*

[b] *School of Energy and Environmental Engineering, Hebei University of Technology, Tianjin 300401, China. E-mail: lianfei2000@126.com; Tel: 86 022 60435775*

[c] *School of Materials Science and Engineering, University of NSW, Kensington, NSW 2052, Australia*

[d] *Electron Microscopy Centre, AIIM Building, Innovation Campus, University of Wollongong, North Wollongong, NSW 2517, Australia*

[e] *Institute for Superconducting and Electronic Materials and School of Physics, University of Wollongong, NSW 2522, Australia*

[f] *Stockbridge School of Agriculture, University of Massachusetts, Amherst, Massachusetts 01003, USA*

† Electronic supplementary information (ESI) available: Selected properties of nano-BC; electrochemical characterization of nano-BC; relationship between Fe content in plaque and the rate of ROL in different rice genotypes; SEM/TEM images of BC–IP composites; results of plate-counting assays. See DOI: **https://doi.org/10.1039/d2en00032f**

"dissolved" and likely contains large portion of ultrafine BC particulates such as BC nanoparticles (nano-BC, sizes within 100 nm). The released nano-BC is known to have higher mobility[11] and surface reactivity[12] than bulk-BC in water/soil systems. For instance, nano-BC was reported to trigger the decomposition of antibiotic resistance genes in the aqueous solution due to the self-generation of free radicals.[13] Nano-BC has high colloidal stability in the aquatic environment due to strong hydration force, the critical coagulation concentration (CCC) of which was up to 700 mmol L^{-1} for Na^+.[14] Thus, nano-BC is very likely to attach to root surfaces of aquatic plants, forming an important root–BC interface to directly affect root reactions with surroundings. Nevertheless, how and to what extent the nano-BC attaches and interacts with root surfaces as well as the role(s) of attached-BC in root metabolism are still unclear.

Aquatic plants (such as rice and cattail) are frequently covered by iron plaque (IP) on their root surfaces as a result of the release of oxygen (O_2) and other oxidants into the rhizosphere.[15] IP is a heterogeneous mixture of iron (Fe) oxides and oxyhydroxides which can offer sorption sites for nutrients and toxic metal(loid)s and plays a critical role in the biogeochemical cycling of elements.[16–18] Thus, exploring the impact of nano-BC on the formation and transformation of IP is of importance to reveal the potential role of nano-BC in the rhizosphere micro-environment. To our best knowledge, few studies have systematically examined the effect of nano-BC on the formation of IP.[19–21] Zheng *et al.* found that the addition of BC into a historically multi-metal contaminated soil enhanced the formation of IP on rice roots.[21] Li *et al.* reported that BC increased the retention of Fe(II) through sorption and thus inhibited the formation of IP.[19] The apparent discrepancies may be partly explained by the variation in BC properties, especially the particle-size dependent mobility, surface charge density, and reactivity. Note that the fine BC (<0.18 mm) more effectively increased the amount of IP on rice roots than the coarse BC (0.5–2.0 mm) reported in a previous study.[21] Recent studies have found that BC is redox-active and its electroactive components such as (hydro)quinone and graphitic structures can participate in abiotic redox reactions.[22–24] The amount and crystallinity of IP are greatly dependent on solution chemistry and rate of oxidation.[25,26] Thus, we hypothesize that nano-BC has a great opportunity to contact with the surfaces of roots and mediate the formation and composition of IP, where the forming mechanisms would be dependent on the redox-active functional groups and/or graphitic structures in nano-BC. Revealing the nexus between BC properties and IP formation is of importance to more precisely guide the agricultural practices of BC and develop novel BC products to boost crop production.

The objective of the present study was to (i) examine the boosting effect of nano-BC on the formation of root IP through hydroponic culture; (ii) characterize the configuration of the newly formed BC–IP complexes; and (iii) quantitatively determine the respective contribution of direct oxidation and electron conductivity derived from nano-BC to the formation of IP. Rice (*Oryza sativa* L.) seedlings grown in the artificial rhizosphere solution was selected as a model aquatic plant. Considering the complexity of naturally occurred IP, the formation of Fe(III) (oxyhydr)oxides, a dominating component in IP, on root surfaces was used as a proxy to stand for the authentic IP in the natural condition. The configuration of the newly formed BC–IP complexes was examined by a suite of *in situ* examining methods and characterization techniques including microelectrodes, cyclic voltammetry, and spectro(micro)scopies.

Materials and methods

Preparation of bulk- and nano-BCs

Rice straw, a typical agricultural biomass waste, was selected as the raw material for BC production. Prior to use, the rice straw was washed, oven-dried at 80 °C, crushed, and then pyrolyzed (10 °C min^{-1}) under an anoxic condition at a desired temperature (400 or 700 °C) for 120 min to obtain typical low- and high-temperature BCs. The obtained BC was manually milled and sieved through a 150 μm mesh. The fractionation of nano-BC from the obtained BC samples was based on a previous procedure[14] and depicted in the ESI† Text S1. The obtained nano-BC was referred to as nano400 and nano700, respectively, according to different charring temperatures. Some selected properties of the nano-BC are provided in Table S1.†

To differentiate the contribution of electron transfer from direct oxidation to the formation of IP, a range of chemically reduced nano-BC was prepared according to previous studies.[27] Vials containing 20 mg of nano-BC were filled with 4 mL of 50 mmol L^{-1} sodium bisulfite solution as reducing agent and were shaken overnight in an anoxic condition. The obtained samples were washed anaerobically several times with deionized (DI) water and stored in a vacuum desiccator before use.

Electrochemical measurements

The electrochemical measurements were conducted in a three-electrode configured cell controlled by the CHI610E Lab platform at room temperature. The mediated electrochemical reduction (MER) and oxidation (MEO) of nano-BCs were determined according to an established setup[28] and presented in the ESI† (Text S2) in detail.

Hydroponic culture and root exudates extraction

Rice (*Oryza sativa* L., Nan Jing No. 9108) seeds were sterilized by 4% (V/V) NaClO and then germinated in a DI water irrigated vermiculite medium. After germination, the seedlings were irrigated with 25% strength of nutrient solution for 2 weeks.[12] The pH of the nutrient solution was adjusted to 6.5 with NaOH and HCl. The seedlings were incubated in a growth chamber, with 12 h photoperiod, 25/20 °C day/night temperature, and 60% relative humidity. After appearance of the third leaflet, uniform seedlings were handpicked, rinsed, and transferred into 6-hole ceramic pots containing 1.5 L of DI water. After 24 h, the roots of rice seedlings were removed from the pots and gently washed with DI water three times. The leached water was also kept in the pots. The collected solutions were immediately filtered (nitrocellulose, 0.45 μm) to remove impurities and plant root residues. The filtrate was stored at −20 °C as a stock solution of root exudates. The total organic carbon (TOC) of the stock solution was 15.8 mg TOC per L measured by a TOC analyzer (TOC-VCPH, Shimadzu). The pH of the stock solution was ~5.3.

Measurement of radial oxygen loss from rice roots

The release of oxygen from aquatic plants can be quantified by the rate of radial oxygen loss (ROL).[29] In this work, ROL rate of rice seedlings was measured using a titanium (Ti)-citrate buffer method with minor modifications.[30] The stock solution of Ti(III)-citrate was prepared in HCl solution under a N_2 atmosphere. The roots of some selected three-leaf rice seedlings were rinsed to remove impurities and then immersed in 50 mL of deoxygenated DI water (one plant per tube). An aliquot of Ti(III)-citrate (5 mL) was pipetted into each tube and the plants were incubated in a growth chamber for 6 h. After that, the Ti(III) concentration in the solutions was measured by a UV-visible spectrophotometer (UV-1800, Shimadzu) at 527 nm. The experiments were performed in triplicate. The rate of ROL (μmol O_2 per g h^{-1}) was calculated by the following formula:

$$\text{Rate of ROL} = \frac{c(y-z)}{gt} \tag{1}$$

where c is the initial volume of Ti(III) solution added to each tube (L), y is the concentration of Ti(III) in the control (without plant) (μmol L^{-1}), z is the final concentration of Ti(III) in the solution with plants (μmol L^{-1}), and g is the root dry weight (g), t is time (h), respectively.

Binding of nano-BC on rice roots

The attachment and later IP formation experiments were performed in an artificial rhizosphere solution (the main composition is listed in Table S2†) to mimic a natural growing condition for rice plants.[31] Uniform seedlings were transplanted into a 1.0 L brown glass bottle containing 500 mL of artificial rhizosphere solution and 10 mg L^{-1} of nano-BC to examine the binding capacity of roots for nano-BC. The dosage of nano-BC was selected based on its estimated natural concentration.[8] The experiment lasted for 24 h and the bottles were gently stirred occasionally to ensure the nano-BC was well suspended. We noted that the apparent equilibrium can be achieved within 24 h. At different time intervals, the suspension was sampled and vacuum-filtered (polyethersulfone, 0.22 μm). The spent membranes were oven-dried at 80 °C to obtain the intercepted mass of nano-BC. The amount of attached nano-BC was calculated as the difference between the added and recovered nano-BC in the suspension. Bottles receiving only artificial rhizosphere solution instead of BC suspension were used as control. All the binding experiments had four replicates. To determine the effects of root vitality and root exudates on the binding of nano-BC, two separate binding experiments were conduct as mentioned above except using differently treated rice seedlings: (i) the root systems of seedlings were thoroughly rinsed by DI water to remove root exudates and then separated from the shoots by severing the stems of seedlings about 2 cm above the surface of aqueous solution. Immediately, the root cross-section was covered by Vaseline to prevent the intrusion of impurities (*i.e.*, severed roots without exudates); (ii) the root systems were just separated from the shoots but without washing by DI water (*i.e.*, severed roots with exudates).

Formation, extraction, and characterization of BC-induced IP from roots

All six seedlings with the same growth were transferred into 500 mL suspension of nano-BC (5.0, 10, or 20 mg L^{-1}) in the artificial rhizosphere solution and followed by the addition of $FeSO_4 \cdot 7H_2O$ stock solution to form IP along root surfaces and cultivated for 2 days, where the final concentration of Fe(II) was 25, 50, and 100 mg L^{-1}, respectively. After harvest, the rice roots were washed thoroughly with DI water. The extraction of IP was conducted according to the dithionite–citrate–bicarbonate method and the extracts were analyzed for Fe by an inductively coupled plasma mass spectrometer (ICP-MS, ICAP-TQ, Thermo).[32] The nano-BC induced IP was characterized utilizing an environmental scanning electron microscope with an energy dispersive X-ray spectroscope (SEM/EDS) (Phenom Prox, ThermoFisher, Netherlands) and a JOEL ARM aberration corrected scanning transmission electron microscope (STEM), energy electron loss spectroscope (EELS), and EDS analyzer. Further details of the methods were reported previously.[33] To examine the impact of nano-BC on microbial assemblage, microbial colonies on IP were enumerated in the presence and absence of nano-BC with plate-counting assays. The detailed methods can be found in the ESI† Text S3.

Dynamics of redox potential and oxygen concentration on root surfaces

A single three-leaf rice seedling was selected and transferred to a ceramic pot (1.5 L) and the roots were fixed with a sponge wrapped clamp. A micromanipulator (MM33-2, Unisense) with microelectrodes was mounted on a lab stand (LS18, Unisense) to avoid shaking during the microelectrode movement and ensure a minimum contact distance (500 μm) between microelectrode and rice roots.[34] Newly formed roots with the same length were selected and measured at a distance of 20 mm from root tips. The O_2 concentration was measured using an O_2 microelectrode (OX-N, Unisense) connected with a picoammeter (PA2000, Unisense). The redox potential was measured using a platinum microelectrode (Rd-N, Unisense) combined with a simple open-ended Ag–AgCl reference electrode (REF, Unisense), and a millivoltmeter was connected to a computer. After incubated approximate 2 h, the redox potential and O_2 on root surfaces were measured every 1 minute and lasted for 48 h.

Fe(II) oxidation induced by nano-BC and root exudates

The experiment was conducted in a 100 mL three necked flask and the openings were used for nitrogen (N_2) inlet/outlet and sampling, respectively. The flask was added with 80 mL of Fe(II) solution and followed by nano-BC suspension, root exudates, and their mixture, respectively, where the final concentration of nano-BC, root exudates, and Fe(II) was 10, 15, and 50 mg L^{-1}. Solutions containing Fe(II) without nano-BC and root exudates were prepared under the same condition as controls. To ensure an anoxic environment, the flask was exerted with N_2 gas (200 mL min^{-1}) during the whole experiment and all the solutions were prepared with deoxygenated DI water. To probe the effect of hydroxyl radical ($^{\bullet}OH$) on the oxidation of Fe(II), another set of experiment was performed under the same conditions except that nano-BC coupled with *tert*-butyl alcohol (TBA) was added. TBA was used as a typical scavenger for $^{\bullet}OH$.[35] The mixture was shaken and sampled at different time intervals. After extraction with 1 mol L^{-1} HCl, the samples were centrifuged (10 000 rpm for 15 min) and filtered (0.22 μm). The concentrations of Fe(II) and Fe(III) in the supernatant were quantified with the ferrozine assay.[36]

Root morphology and nutrient concentrations of plants

To examine the negative effect of excess nano-BC on rice seedlings growth, a larger range of nano-BC concentrations (0–80 mg L^{-1}) was selected to carry out the hydroponic culture of rice seedlings in 500 mL artificial rhizosphere solution as mentioned above. After harvest, the root morphologies including accumulative root length, surface area, volume, average diameter, number of root tips and crossings were analyzed using the WinRhizo system v. 4.0b (Regent, Canada) for the rice plants with IP induced by different dosages of nano-BC. After harvesting, rice shoots and roots were dried in the oven at 70 °C for 48 h, and then ground into fine powder. The fine powder (100 mg) was digested with H_2SO_4 and H_2O_2. Then, the total concentrations of N and P in the dried shoots and roots were measured by a continuous flow analyzer (SEAL Auto Analyzer AA3, GER) at 660 and 700 nm, respectively. While those of other selected elements including K, Ca, Mg, Mn, S, Cu, Fe, and Zn were detected by ICP-MS. Briefly, the dried tissues (50 mg) were digested (190 °C, 30 min) in a microwave accelerated reaction system (CEM Corp., Matthews, NC) with a mixture of HNO_3 (3 mL) and ultrapure water (v/v = 1 : 1). The digested solution was passed through a 0.22 μm filter and diluted to 50 mL by using ultrapure water (Milli-Q) for ICP-MS analysis.

Quantitative real-time polymerase chain reaction

Root samples treated by different dosages of nano-BC were ground with liquid N_2 and total RNA was extracted using Takara MiniBEST Plant RNA Extraction Kit (Takara, Japan). Reverse transcription was conducted using an EasyQuick RT MasterMix (CWBIO, China) in a thermal cycler (T100™; Bio-Rad, Singapore). Quantitative real-time polymerase chain reaction (qPCR) was performed using UltraSYBR Mixture (CWBIO, China) in a thermal cycler (C1000 Touch™; Bio-Rad, Singapore) equipped with a real-time PCR detection system (CFX96™; Bio-Rad). OsAct1 (National Center for Biotechnology Information accession number: XM_015777404) was used as an internal reference gene.[37] Each PCR reaction tube (25 μL of UltraSYBR mixture) contained 1 μL each of the forward and reverse primers (at a final concentration of 0.2 μM), 21 μL of RNase-free water, and 2 μL first-strand cDNA of each sample. The thermal program of qRT-PCR amplification was 95 °C for 30 s, followed by 40 cycles of 95 °C for 15 s and 60 °C for 30 s. Relative gene expressions were calculated using the $2^{-\Delta\Delta CT}$ methods.

Results and discussion

Attachment of nano-BC on rice roots

For better understanding the role of nano-BC in the formation of IP, it is crucial to examine the binding capacity of nano-BC on rice roots. Our data show that up to 6.0% of suspended nano-BC can attach to the rice root surfaces within 24 h (Fig. 1a and b). Comparatively, higher amount of nano400 was entrapped by roots relative to nano700, probably due to its higher content of O-containing groups (Table S1†) and polar nature.[14] To examine how the physiological activity of rice seedlings affected the binding of nano-BC, the rice roots were divided into three groups, *i.e.*, intact roots, severed roots with exudates, and severed roots without exudates. We noted that the intact roots exhibited higher ($p < 0.05$) binding capacity for nano-BC than the severed roots, implying that the attachment of nano-BC was closely related to root vitality. The high root vitality of intact roots was reflected by the higher release of O_2 than the severed roots during a period of 48 h (Fig. S1†). Meanwhile, the severed roots with root exudates adsorbed more nano-BC than those without root exudates. The results suggest that the growth status and root mucilage of plants greatly contributed to the entrapment of nano-BC by roots. The microscope images visually demonstrate the attachment of nano-BC by rice roots. It is evident that more nano-BCs were associated with the relatively young roots than the old ones (Fig. 1c and d), which supported the importance of root vitality for the binding of nano-BC. Meanwhile, root hairs might also play a crucial role in the entrapment of nano-BC (Fig. 1e and f). These observations imply that nano-BC is more likely to attach other than passively deposit onto the root surfaces.

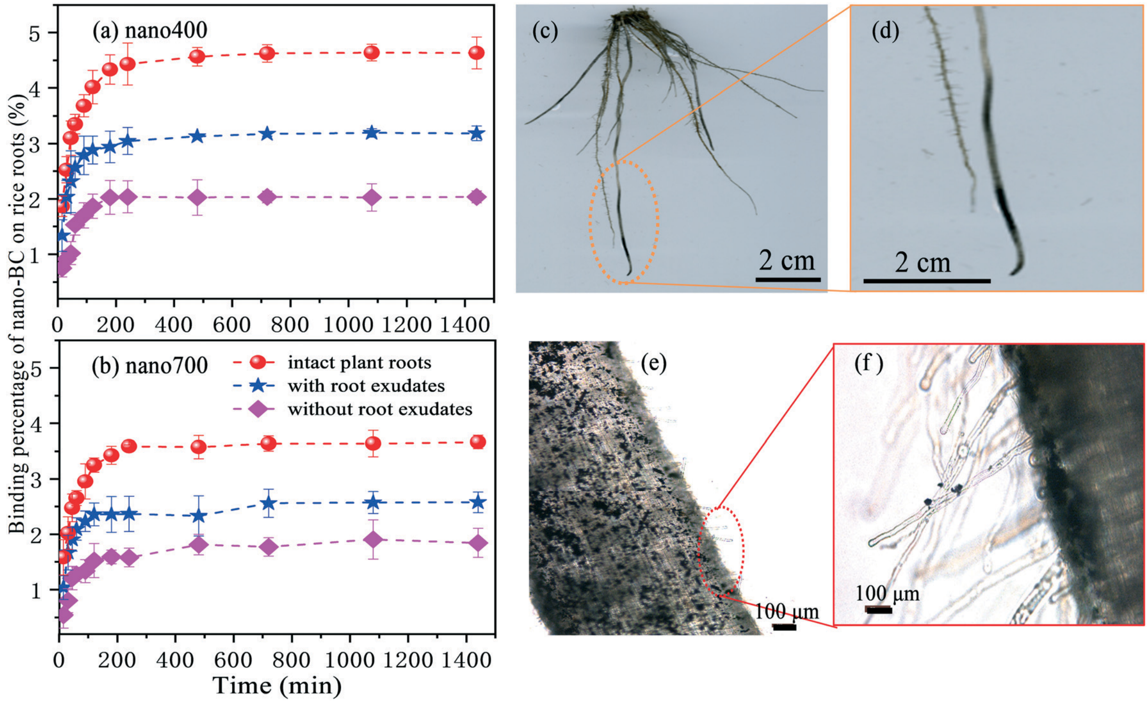

Fig. 1 Attachment of nano-BC (nano400 and nano700) on intact rice plant roots, severed roots with exudates, and severed roots without exudates. (a) nano400; (b) nano700; (c–f) microscope images of attached nano-BC on root surfaces.

Nano-BC induced formation of root IP

We explored the effect of nano-BC on the formation of IP in the presence of Fe(II) (Fig. 2a and b). The content of Fe in the IP increased with increasing dosage of nano-BC and peaked at 10 and 5.0 mg L^{-1} for nano400 and nano700, respectively. A similar trend was observed for all other concentrations of Fe(II) (25–100 mg L^{-1}) in the aqueous solution, indicating that the positive effect of nano-BC on the formation of IP was relatively stable in a wide range of Fe(II) concentrations. It is well known that the formation of IP is highly dependent on the magnitude of O_2 released from roots in the anoxic environment.[38] The excess O_2 enables soluble Fe(II) to be oxidized to form Fe(III)-(oxyhydr)oxides. Besides O_2, we hypothesize that the attached nano-BC could also induce the oxidization of Fe(II) because of its relatively high catalytic ability.[23] To test the hypothesis, the dynamics of redox potential and O_2 concentration on root surfaces within 48 h were measured using microelectrodes before and after binding with nano-BC (Fig. 2c–f). Note that the highest value of redox potential and O_2 concentration appeared when the dosage of nano400 and nano700 reached to 10 and 5.0 mg L^{-1}, respectively. At higher nano-BC dosages, however, both the oxidation potential and O_2 concentration decreased gradually, which was consistent with the trend of Fe content in IP. The results suggest that the formation of IP was highly dependent on the attached nano-BC, which probably mediated the redox potential and/or oxygen secretion at root surfaces. Meanwhile, the excess nano-BC was unfavorable to plant growth (see more discussion below).

The nano-BC in this study was redox-active reflected by the high reductive and oxidative currents in MER and MEO, respectively (Fig. S2a†). Comparatively, nano700 possessed faster electron transfer kinetics than nano400 suggested by its sharper current peaks. Integration of the current peaks yielded the values of electron accepting capacities (EAC) of nano-BCs (*i.e.*, 1.7 mmol e^{-} g^{-1} and 1.9 mmol e^{-} g^{-1} for nano400 and nano700, respectively), higher than their bulk counterparts (1.0 mmol e^{-} g^{-1} and 1.2 mmol e^{-} g^{-1}, respectively) (Fig. S2b†) and also slightly higher than that of 500 °C wood BC in the literature,[28] implying their oxidative nature. Thus, the attached nano-BC was electrochemically favorable to the formation of IP. If nano-BC was the foremost factor in regulating the Fe(II) oxidation, the content of Fe in IP would have been increased at higher dosage of nano-BC. However, the opposite was observed (Fig. S3†). This paradox made it necessary to further identify the respective contribution of nano-BC and O_2 to the formation of IP. To this end, as many as 6 other rice genotypes were cultivated simultaneously under the same hydroponic condition and the relationship between ROL rates and Fe content in IP was examined in the presence and absence of nano-BC, respectively (Fig. S4†). We found that (i) the Fe content in IP was positively correlated with the rate of ROL no matter with and without nano-BC; and (ii) the presence of nano-BC greatly contributed to the increase of Fe content in IP for all the tested genotypes. The data suggested that the secreted O_2 played a more crucial role in the formation of IP than nano-BC; while the attached nano-BC could assist in the oxidation of Fe(II). However, when excessive nano-BC attached to rice

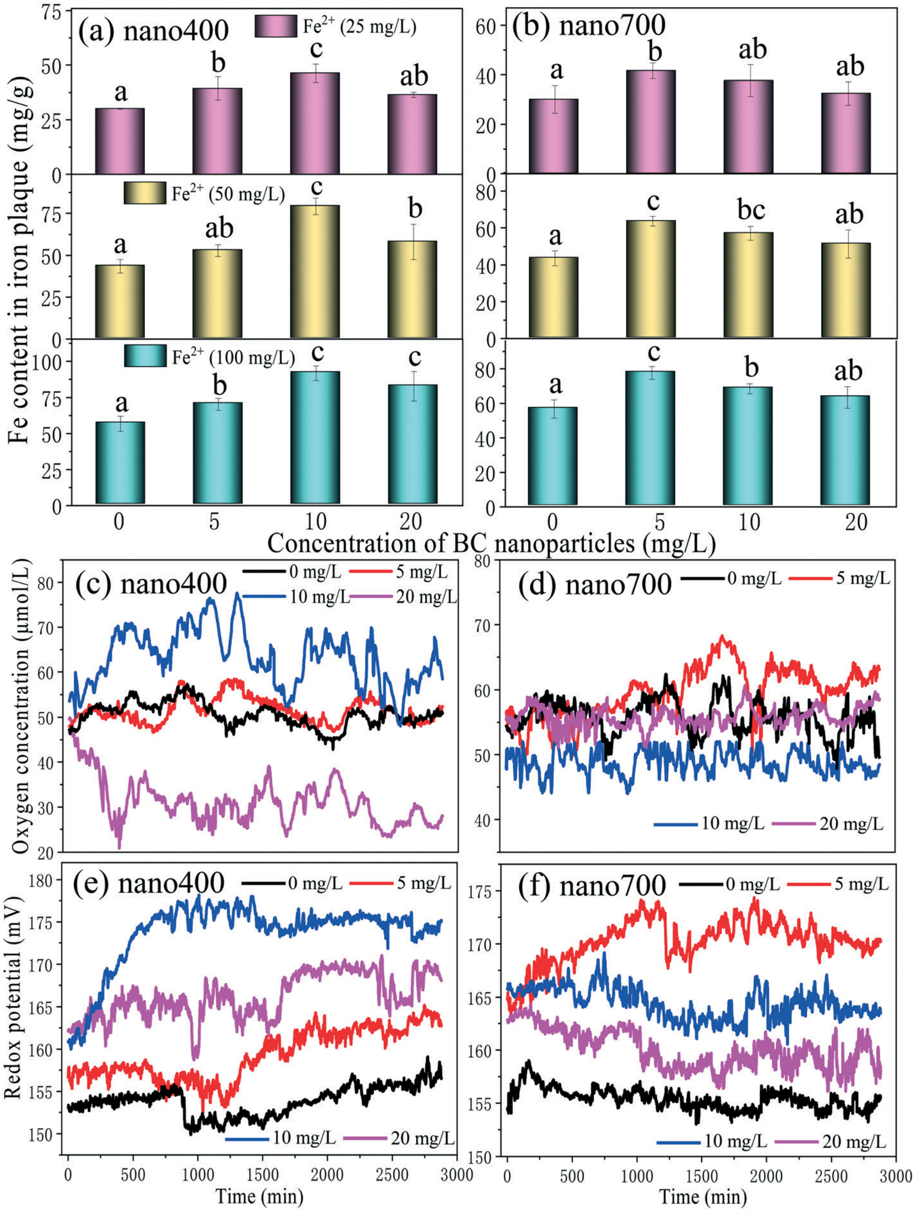

Fig. 2 Effect of nano-BC (nano400 and nano700) on Fe content in iron plaque newly formed on rice roots in the presence of soluble Fe(II) with various concentrations (25, 50, and 100 mg L^{-1}), respectively (a and b). Oxygen concentration and redox potential profiles of rice roots treated by different concentrations of nano-BC over a period of 48 h (c–f). Different letters represent different statistical groups suggested by the Tukey-HSD multiple comparisons at $p < 0.05$.

roots, it might partially inhibit the oxygen secretion by blocking aerenchyma and negatively affect the metabolism of rice plants due to its high surface reactivity, thus obstructing the formation of IP. Our recent study also noticed that the addition of 100 mg L^{-1} nano-BC produced at 600 °C caused oxidative stress to rice seedlings reflected by the significantly increased contents of antioxidative enzyme activities.[12]

Unique configuration of nano-BC induced IP

Root surfaces without the binding of nano-BC comprised a relatively uniform nonporous plaque layer, which was surrounded by root hairs and probably fungi revealed by SEM and 3D topographical mapping (Fig. S5†). Our SEM images show that the plaque layer was fairly regular with the thickness around 30 μm. By contrast, micron-sized BC particles were identified on root surfaces after the addition of 5 mg L^{-1} nano400 in the suspension (Fig. 3a), where the BC particles exhibited at least two association patterns with IP; *i.e.*, embedded in and on the plaque layer. In the first pattern (Fig. 3b), the BC particles lied on the IP, covered by a layer of organic compounds and minerals rich in Fe, Si and P covering its surface. In the second pattern (Fig. 3c), the BC particles stood on the plaque layer, where high contents of

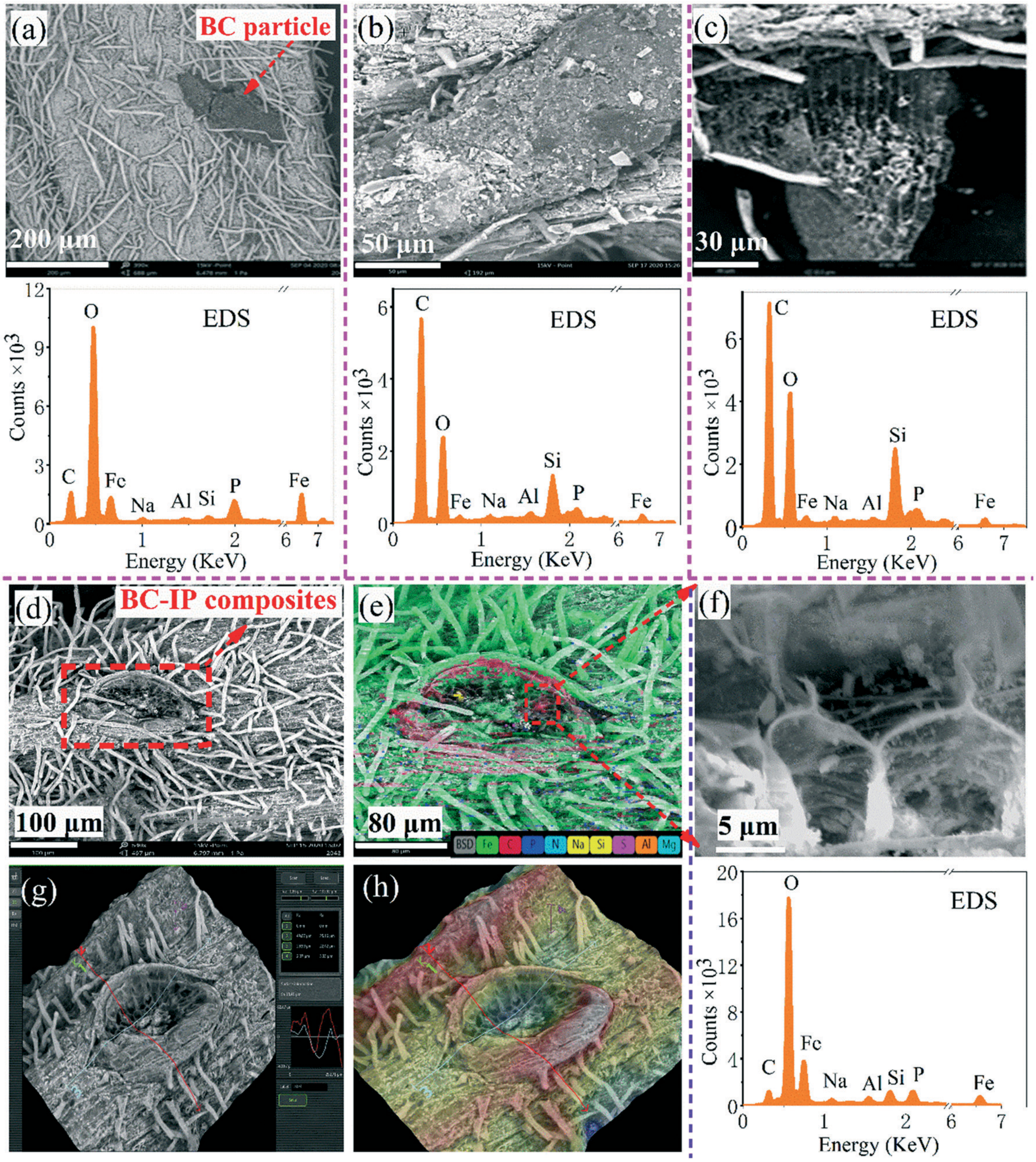

Fig. 3 Spectro(micro)scopic characterization of iron plaque–BC composites on the rice root surfaces. SEM images and EDS of root surfaces embedded with nano400 (a–c) or nano700 (d and e); (f) higher magnification of the porous area in panel (e) identifying the presence of organomineral-agglomerates in the pores; and 3D topographical maps of root surfaces embedded with nano700 (g and h). The concentration of nano-BC in the suspension was 5.0 mg L^{-1}.

Si, Na, Al, P, and Fe were found on its surfaces. Moreover, the presence of relatively high concentrations of N and S indicated microorganisms growing in the pores (Fig. S6†). 3D topographical maps (Fig. S7†) indicate that the thickness (30–60 μm) and roughness of the nano-BC induced IP were greater than that of control (Fig. S5†).

Comparatively, the composites of nano700-IP exhibit a distinct surface morphology, where nano700 was more porous relative to nano400 and an evident plaque layer can be found around BC surfaces (Fig. 3d and e). The high magnification image of the pores shows that they were filled with a range of organomineral-agglomerates consisting of Fe, Si, P, Al, and Na (Fig. 3f). It is more clear from the 3D maps (Fig. 3g and h) that the edges of BC particles were surrounded by a thick IP (~60 μm) while some central macropores were uncovered by IP forming a basin-like structure, which indicates that more active sites were probably located on the edges of BC.[39]

Needle like structures were observed by STEM on the epidermal layer of control roots (Fig. 4a and b) and around

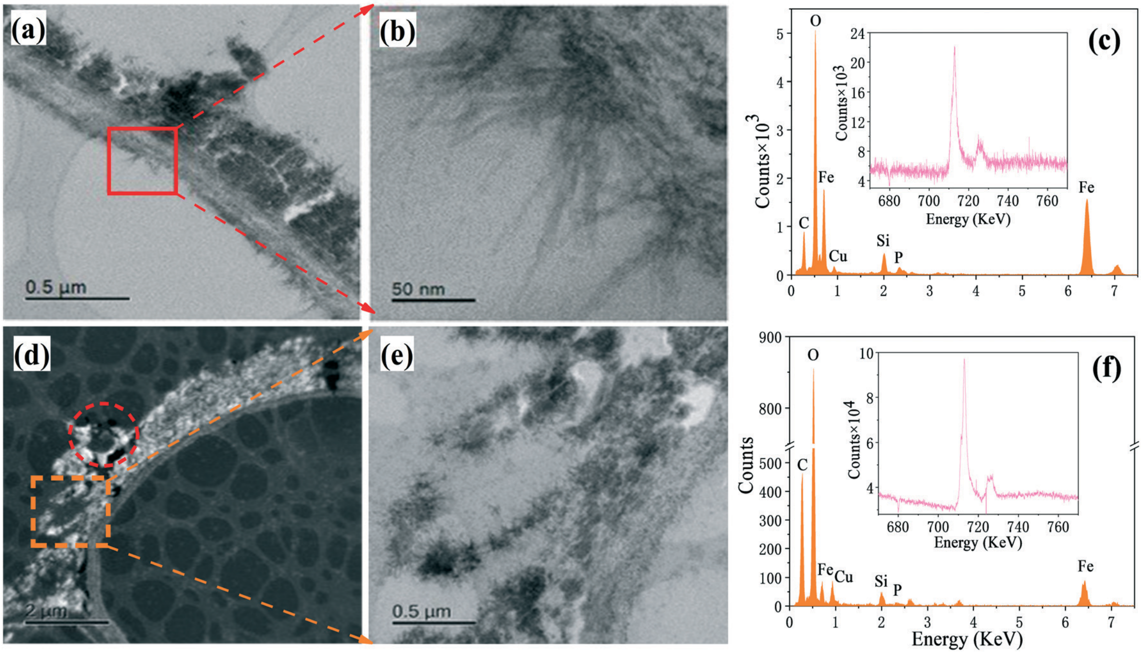

Fig. 4 STEM images and EDS spectra of control roots (a–c) and nano-BC attached roots (d–f). The insets in panels (c) and (f) are EELS spectra inside the red and orange squares, respectively. The orange square in panel (d) highlights a bacterium with a coating of Fe/O needle-like structures on the surface and inside; the red circle shows an attached BC particle as indicated by EELS and EDS.

bacteria in the plaque layer of the root (Fig. 4d and e). EDS analysis showed that the needles had a high concentration of Fe, O and a smaller amount of Si. Comparison with the shape and the energy loss of the Fe $L_{2,3}$ edge indicates that the iron oxide is magnetite as given in the reference spectra reported in ref. 33. The EELS spectrum of the needle like structure inside the epidermal layer (Fig. S8†) indicated that the needles could also contain maghemite or magnetite.[40] For the nano-BC attached roots (Fig. 4d–f), besides needle like Fe(III) (oxyhydr)oxides, micron sized BC particles were found to be located in the plaque layer. More interestingly, the surfaces of BC were surrounded by Fe/O nanoparticles, which were mainly composed of $Fe_3(PO_4)_2$ and/or hematite as indicated by EDS and EELS. Generally, biomass-derived BC contains certain amount of P especially that from manure[41] and bonemeal,[42] which would play a potential role in the deposition and redox reactions occurred on BC surfaces. Moreover, BC has a high sorption affinity for PO_4^{3-} from aqueous solutions through precipitation and/or surface deposition.[43] Thus, the Fe/P/O enriched nanoparticulates on BC-induced IP might be mainly attributed to the precipitation of Fe with PO_4^{3-}. Also, more bacteria were found on the plaque layer and very close to the BC particles relative to the control (Fig. 4d and e). To further demonstrate the nano-BC induced assemblage of microorganisms on IP, plate-counting assays were conducted, which indicated that the concentrations of microorganisms in the nano-BC treatments were at least two times higher than that of control (Fig. S9†). However, the impact of nano-BC on the activity of bacteria on IP is still largely unknown, which might be related to the aggregation of cells with BC surfaces[24] and nano-BC facilitated electron transfer.[44] These results indicate that the attached nano-BC can be considered as active sites not only for the formation of IP on rice root surfaces but also for the colonization of microorganisms, which merits further investigations such as electron transfer efficiency driven by nano-BC. These observations indicate that the newly formed BC–IP mixture possessed an unique structure, where both poorly crystalline Fe(III) (oxyhydr)oxides and Fe-containing nanoparticles can be developed on BC surfaces.

Mechanisms of IP formation induced by nano-BC

The oxidizing capacity of both original and TBA (scavenger for $^{\bullet}OH$)-treated nano-BCs for Fe(II) in the presence and absence of root exudates was examined under anoxic conditions. As shown in Fig. 5a, ~7.0% and 9.0% of Fe(II) in the aqueous solution were oxidized by the original nano400 and nano700, respectively. A fraction of Fe(II) can also be oxidized (~3.0%) by root exudates due to the presence of oxidants secreted from rice roots (*e.g.*, H_2O_2). When nano-BC and root exudates existed simultaneously in the reacting system, the oxidization of Fe(II) was enhanced to 11.2% and 13.4% for nano400 and nano700, respectively, indicating their additive effect on the formation of IP. However, similar to the control (without nano-BC and root exudates), negligible Fe(II) can be oxidized by the TBA-treated nano-BCs due to the remarkably decreased oxidizing capacity of nano-BCs as suggested by the significant decrease of oxidative currents with increasing TBA concentrations (Fig. S10†). The results indicated that the oxidizing capacity of nano-BCs was

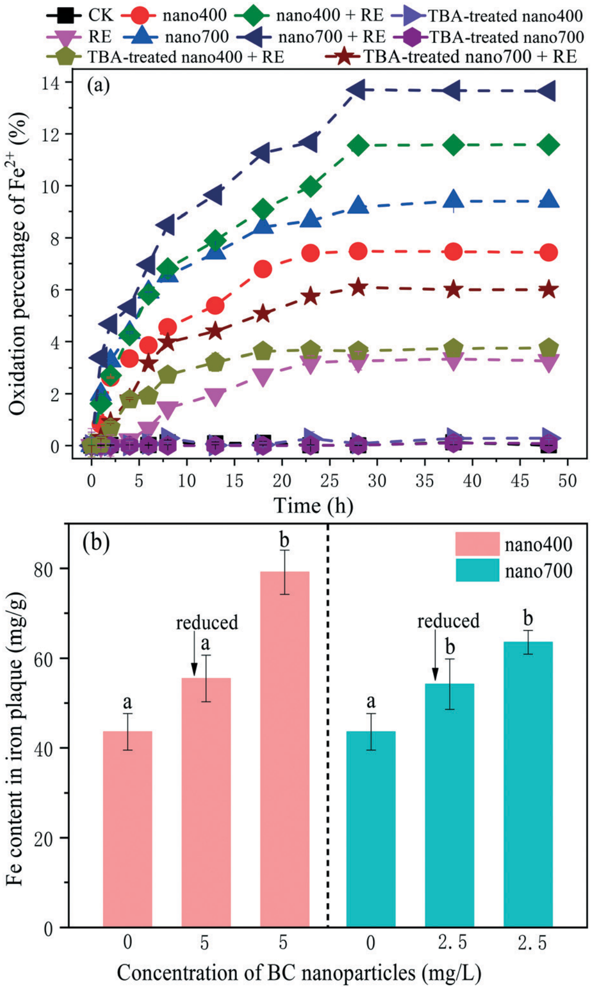

Fig. 5 Oxidation percentage of Fe(II) in aqueous solutions in the presence of nano-BC (nano400 and nano700), root exudates (RE), mixture of nano-BC and RE, TBA-treated nano-BC, as well as mixture of TBA-treated nano-BC and RE, respectively (a); Fe content in the iron plaque on root surfaces affected by pristine and chemically reduced nano-BC, respectively (b). The concentration of TBA in the suspension was 60 and 80 μmol L^{-1} for nano400 and nano700, respectively, based on the voltammetric analyses in Fig. S8.† Different letters represent different statistical groups suggested by the Tukey-HSD multiple comparisons at $p < 0.05$.

largely derived from the reactive oxygen species (*e.g.*, $^{\bullet}OH$) generated during the carbonization of BC.[45]

Note that the addition of root exudates differently recovered the oxidizing capacity of TBA-treated nano400 and nano700. For the nano400-exudates combination, the oxidation percentage of Fe(II) increased to 3.76%, similar to 3.26% oxidized by root exudates alone, indicating the negligible contribution of TBA-treated nano400 to the oxidization of Fe(II). Conversely, for the nano700-exudates combination, the oxidation percentage of Fe(II) was up to 6.01%, almost two times higher than that in the case of only root exudates existed, suggesting that besides root exudates nano700 greatly contributed to the oxidization of Fe(II). This large gap can be explained by the distinct electrochemical feature of nano700 relative to nano400. It has been reported that conjugated aromatic sheets in BC can grow large enough to achieve electron conductivity when the heat treatment temperature is higher than 600 °C.[28,46] However, the high temperature would concomitantly decrease the content of oxyl groups on BC. Thus, the catalytic ability of nano400 and nano700 mainly stemmed from the redox-active moieties and graphitic structures, respectively.[23,28] In contrast to the (hydro)quinones, graphitic structures are more like an electron shuttle between electron donor and acceptor. The increased Fe(II) oxidation by the mixture of nano700 and root exudates was probably caused by the nano700-mediated electron transfer reactions between Fe(II) and oxidants (such as secreted O_2 and H_2O_2) in root exudates. The cyclic voltammetric results (Fig. S2†) also illustrated the higher electron transfer efficiency of nano700. Consistently, an increasing number of studies have found that BC materials, especially high-temperature ones, could accelerate electron transfer from minerals to bacteria[3,24] and from nucleophiles (*e.g.*, sulfides) to nitrocompounds.[46] Moreover, BC was demonstrated to have a high adsorption capacity for divalent cations,[3] which could potentially increase the electron transfer efficiency. By contrast, the relative low electron conductivity of nano400 greatly limited its involvement in this type of Fe(II) transformation.

To further quantify the respective contribution of direct oxidation and electron transfer to the formation of IP, the effect of chemically reduced nano-BC on the forming of IP was examined (Fig. 5b). For nano400, the chemically reduced sample did not significantly ($p > 0.05$) increase the formation of IP compared to the control. For nano700, however, the reduced sample significantly ($p < 0.05$) increased the formation of IP similar to the pristine BC, indicating the more important role of electron transfer than direct oxidation in the transformation of Fe(II). It can be calculated from Fig. 5b that the direct oxidation accounted for ~70% to the formation of IP for nano400, while the electron transfer accounted for at least 55% in the case of nano700 in the present study.

Rice responses to excess nano-BC burden

Excess nano-BC not only impeded the formation of IP but was detrimental to plant growth as reflected by a number of critical indexes (*i.e.*, height and dry weight, root morphology, nutrient contents of rice seedlings, and gene expression). Comparing the panels in Fig. 2, the plant height, dry weight (roots and shoots), and root morphologies including tips, length, surface area followed the same trend with increasing nano-BC dosage, *i.e.*, they increased initially to reach peaks at 10 or 5.0 mg L^{-1} for nano400 and nano700, respectively, and then dropped with higher nano-BC dosages (Fig. 6a–d). Consistently, the concentrations of selected nutrient elements (N, P, K, Ca, Mg, Mn, S, Cu, Fe, Zn) in roots and shoots also peaked at the critical nano-BC dosages (10 or 5.0 mg L^{-1}) and then significantly decreased ($p < 0.05$) when

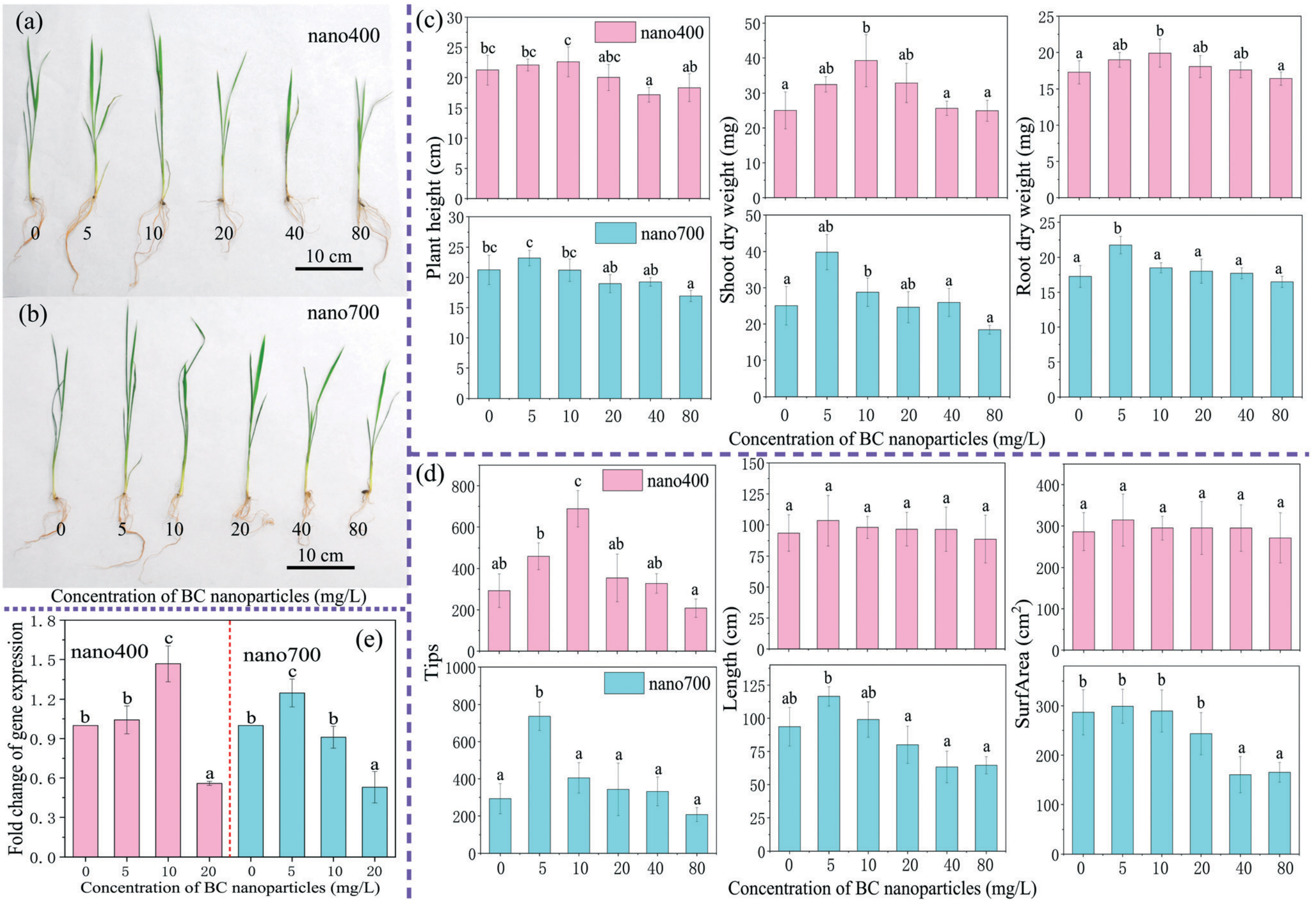

Fig. 6 The effect of different concentrations of nano-BC (nano400 and nano700) on rice plant height, dry weight (roots and shoots) (a–c), root morphologies including tips, length, surface area (d), and iron transport related gene (*OsFRDL1*) relative express (e). Different letters represent different statistical groups suggested by the Tukey-HSD multiple comparisons at $p < 0.05$.

excess nano-BC was added (Tables S3 and S4†). The excess nano-BC might cover a large portion of root surfaces and consequently decrease the release of O_2 and root exudates as well as the nutrient uptake by blocking the ion channels.[12] Additionally, the higher BC burden might increase the risk of oxidation damages originating from persistent free radicals in BC.[47]

To explore the negative effect on plant growth from the genetic level, a qPCR assay on a well-recognized iron transport related gene (*OsFRDL1*)[37] was performed (Fig. 6e). *OsFRDL1* plays an important role in the efficient translocation of Fe from rice roots to shoots. Compared with the control, *OsFRDL1* was significantly upregulated ($p < 0.05$) when treated by 10 mg L^{-1} of nano400 or 5.0 mg L^{-1} of nano700; while that was downregulated by ~2.5-fold when the concentration of nano-BC increased to 20 mg L^{-1}. The gene expression data indicate that *OsFRDL1* might be impaired in the rice plants subjected to excess dosage of nano-BC. Meanwhile, it is reasonable to believe that besides *OsFRDL1* other genes responsible for nutrient uptake and/or transport are also likely to be damaged by the higher loading of nano-BC considering the lowered plant growth and nutrient concentrations as mentioned above.

Conclusions

Our results illustrate that the formation of root IP in aquatic plants is highly dependent on the redox properties of attached nano-BC. We for the first time quantitatively demonstrate that direct oxidation of aqueous Fe(II) and electron transfer from Fe(II) to oxidants in root exudates are the dominating mechanisms for the enhanced formation of IP induced by low- and high-temperature nano-BC, respectively. The newly formed BC–IP complex has higher porosity and roughness relative to the common plaque layer. Both poorly crystalline Fe(III) (oxyhydr)oxides and Fe-containing nanoparticles were developed on the surfaces of BC–IP complex. Additionally, more microorganisms were observed on the new plaque layer than on the common IP in control suggests that besides abiotic oxidation of Fe(II) the attached nano-BC may play a critical role in the colonization and adaptive evolution of microorganisms on BC–root interfaces. Thus, the biotic contribution to the development of BC–IP composites on roots merits further investigations. The results in the present study help us to better understanding the role of suspended nano-BC in the formation of root IP, growth of aquatic plants, and redox-driven elemental cycles in the water–root interfaces.

Conflicts of interest

There are no conflicts to declare.

Acknowledgements

Financial supports were provided by the National Natural Science Foundation of China (41977278, 41573127, 41820104009), Jiangsu Agricultural Science and Technology Innovation Project (CX(20)3080), and the Fundamental Research Funds for the Central Universities (JUSRP22015). We thank Paul Munroe from School of Materials Science and Engineering, University of NSW, Yiwen Wang from the School of Life Sciences, East China Normal University, and Guanghong Chen from Guangdong Institute of Eco-Environmental Science & Technology, China for their assistance in the characterization of nano-BC and BC–IP composites.

References

1 L. Beesley, E. Moreno-Jimenez and J. L. Gomez-Eyles, Effects of biochar and greenwaste compost amendments on mobility, bioavailability and toxicity of inorganic and organic contaminants in a multi-element polluted soil, *Environ. Pollut.*, 2010, **158**, 2282–2287.

2 F. P. Vaccari, S. Baronti, E. Lugato, L. Genesio, S. Castaldi, F. Fornasier and F. Miglietta, Biochar as a strategy to sequester carbon and increase yield in durum wheat, *Eur. J. Agron.*, 2011, **34**, 231–238.

3 S. Xu, D. Adhikari, R. Huang, H. Zhang, Y. Tang, E. Roden and Y. Yang, Biochar-facilitated microbial reduction of hematite, *Environ. Sci. Technol.*, 2016, **50**, 2389–2395.

4 M. W. Jones, C. Santín, G. R. van der Werf and S. H. Doerr, Global fire emissions buffered by the production of pyrogenic carbon, *Nat. Geosci.*, 2019, **12**, 742–747.

5 Y. Fang, Y. Chen, G. Huang, L. Hu, C. Tian, J. Xie, J. Lin and T. Lin, Particulate and dissolved black carbon in coastal china seas: spatiotemporal variations, dynamics, and potential implications, *Environ. Sci. Technol.*, 2020, **55**, 788–796.

6 S. Wagner, J. Brandes, R. G. M. Spencer, K. Ma, S. Z. Rosengard, J. M. S. Moura and A. Stubbins, Isotopic composition of oceanic dissolved black carbon reveals non-riverine source, *Nat. Commun.*, 2019, **10**, 5064.

7 S. Wagner, R. Jaffé and A. Stubbins, Dissolved black carbon in aquatic ecosystems, *Limnol. Oceanogr. Lett.*, 2018, **3**, 168–185.

8 R. Jaffé, Y. Ding, J. Niggemann, A. V. Vähätalo, A. Stubbins, R. G. Spencer, J. Campbell and T. Dittmar, Global charcoal mobilization from soils via dissolution and riverine transport to the oceans, *Science*, 2013, **340**, 345–347.

9 X. Qu, H. Fu, J. Mao, Y. Ran, D. Zhang and D. Zhu, Chemical and structural properties of dissolved black carbon released from biochars, *Carbon*, 2016, **96**, 759–767.

10 J. A. Roebuck Jr, M. Seidel, T. Dittmar and R. Jaffé, Land use controls on the spatial variability of dissolved black carbon in a subtropical watershed, *Environ. Sci. Technol.*, 2018, **52**, 8104–8114.

11 W. Yang, J. Shang, B. G. Li and M. Flury, Surface and colloid properties of biochar and implications for transport in porous media, *Crit. Rev. Environ. Sci. Technol.*, 2020, **50**, 2484–2522.

12 L. Yue, F. Lian, Y. Han, Q. Bao, Z. Y. Wang and B. S. Xing, The effect of biochar nanoparticles on rice plant growth and the uptake of heavy metals: Implications for agronomic benefits and potential risk, *Sci. Total Environ.*, 2019, **656**, 9–18.

13 F. Lian, W. Yu, Q. Zhou, S. G. Gu, Z. Y. Wang and B. S. Xing, Size matters: nano-biochar triggers decomposition and transformation inhibition of antibiotic resistance genes in aqueous environments, *Environ. Sci. Technol.*, 2020, **54**, 8821–8829.

14 F. Lian, W. Yu, Z. Y. Wang and B. S. Xing, New insights into black carbon nanoparticle-induced dispersibility of goethite colloids and configuration-dependent sorption for phenanthrene, *Environ. Sci. Technol.*, 2019, **53**, 661–670.

15 R. F. Chen, R. F. Shen, P. Gu, X. Y. Dong, C. W. Du and J. F. Ma, Response of rice (Oryza sativa) with root surface iron plaque under aluminium stress, *Ann. Bot.*, 2006, **98**, 389–395.

16 D. C. Amaral, G. Lopes, L. R. Guilherme and A. L. Seyfferth, A new approach to sampling intact Fe plaque reveals Si-induced changes in Fe mineral composition and shoot as in rice, *Environ. Sci. Technol.*, 2017, **51**, 38–45.

17 C. M. Hansel, S. Fendorf, S. Sutton and M. Newville, Characterization of Fe plaque and associated metals on the roots of mine-waste impacted aquatic plants, *Environ. Sci. Technol.*, 2001, **35**, 3863–3868.

18 M. Maisch, U. Lueder, A. Kappler and C. Schmidt, From plant to paddy—how rice root iron plaque can affect the paddy field iron cycling, *Soil Syst.*, 2020, **4**, 28.

19 J. Li, S. L. Wang, J. Zhang, L. Zheng, D. Chen, Z. Wu, S. M. Shaheen, J. Rinklebe, Y. S. Ok, H. Wang and W. Wu, Coconut-fiber biochar reduced the bioavailability of lead but increased its translocation rate in rice plants: Elucidation of immobilization mechanisms and significance of iron plaque barrier on roots using spectroscopic techniques, *J. Hazard. Mater.*, 2020, **389**, 122117.

20 J. Y. Zhang, H. Zhou, J. F. Gu, F. Huang, W. J. Yang, S. L. Wang, T. Y. Yuan and B. H. Liao, Effects of nano-Fe_3O_4-modified biochar on iron plaque formation and Cd accumulation in rice (Oryza sativa L.), *Environ. Pollut.*, 2020, **260**, 113970.

21 R. L. Zheng, C. Cai, J. H. Liang, Q. Huang, Z. Chen, Y. Z. Huang, H. P. H. Arp and G. X. Sun, The effects of biochars from rice residue on the formation of iron plaque and the accumulation of Cd, Zn, Pb, As in rice (Oryza sativa L.) seedlings, *Chemosphere*, 2012, **89**, 856–862.

22 A. Kappler, M. L. Wuestner, A. Ruecker, J. Harter, M. Halama and S. Behrens, Biochar as an electron shuttle between bacteria and Fe(III) minerals, *Environ. Sci. Technol. Lett.*, 2014, **1**, 339–344.

23 M. S. Jovita, H. Y. Yu and C. C. Pei, Wood-derived black carbon (biochar) as a microbial electron donor and acceptor, *Environ. Sci. Technol. Lett.*, 2016, **3**, 62–66.

24 Z. Yang, T. Sun, E. Subdiaga, M. Obst, S. B. Haderlein, M. Maisch, R. Kretzschmar, L. T. Angenent and A. Kappler, Aggregation-dependent electron transfer via redox-active biochar particles stimulate microbial ferrihydrite reduction, *Sci. Total Environ.*, 2020, **703**, 135515.

25 C. Wu, Z. H. Ye, H. Li, S. C. Wu, D. Deng, Y. G. Zhu and M. H. Wong, Do radial oxygen loss and external aeration affect iron plaque formation and arsenic accumulation and speciation in rice, *J. Exp. Bot.*, 2012, **63**, 2961–2970.

26 X. J. Yang, Z. Xu and H. Shen, Drying-submergence alternation enhanced crystalline ratio and varied surface properties of iron plaque on rice (Oryza sativa) roots, *Environ. Sci. Pollut. Res.*, 2018, **25**, 3571–3587.

27 X. Zhang, J. Xia, J. Pu, C. Cai, G. W. Tyson, Z. Yuan and S. Hu, Biochar-mediated anaerobic oxidation of methane, *Environ. Sci. Technol.*, 2019, **53**, 6660–6668.

28 L. Kluepfel, M. Keiluweit, M. Kleber and M. Sander, Redox properties of plant biomass-derived black carbon (biochar), *Environ. Sci. Technol.*, 2014, **48**, 5601–5611.

29 W. Armstrong, Aeration in higher plants, in *Advances in Botanical Research*, Academic Press, 1980, vol. 7, pp. 225–332.

30 C. Wu, Z. Ye, W. Shu, Y. Zhu and M. Wong, Arsenic accumulation and speciation in rice are affected by root aeration and variation of genotypes, *J. Exp. Bot.*, 2011, **62**, 2889–2898.

31 C. F. Kerl, T. B. Ballaran and B. Planer-Friedrich, Iron plaque at rice roots: no barrier for methylated thioarsenates, *Environ. Sci. Technol.*, 2019, **53**, 13666–13674.

32 M. Otte, I. Dekkers, J. Rozema and R. A. Broekman, Uptake of arsenic by Aster tripolium in relation to rhizosphere oxidation, *Can. J. Bot.*, 1991, **69**, 2670–2677.

33 J. R. Araujo, L. Van Zwieten, J. Horvat, A. Enders and S. Joseph, Nanoscale analyses of the surface structure and composition of biochars extracted from field trials or after co-composting using advanced analytical electron microscopy, *Geoderma*, 2017, **294**, 70–79.

34 Y. Li and X. Wang, Root-induced changes in radial oxygen loss, rhizosphere oxygen profile, and nitrification of two rice cultivars in Chinese red soil regions, *Plant Soil*, 2013, **365**, 115–126.

35 J. Yang, B. Pan, H. Li, S. Liao, D. Zhang, M. Wu and B. S. Xing, Degradation of p-nitrophenol on biochars: Role of persistent free radicals, *Environ. Sci. Technol.*, 2016, **50**, 694–700.

36 A. Katja, B. Thomas and A. Kappler, Influence of humic acid imposed changes of ferrihydrite aggregation on microbial Fe(III) reduction, *Geochim. Cosmochim. Acta*, 2012, **85**, 326–341.

37 K. Yokosho, N. Yamaji, D. Ueno, N. Mitani and J. F. Ma, OsFRDL1 is a citrate transporter required for efficient translocation of iron in rice, *Plant Physiol.*, 2009, **149**, 297–305.

38 Z. Xu, X. Xu, X. Tao, C. Yao, D. C. W. Tsang and X. D. Cao, Interaction with low molecular weight organic acids affects the electron shuttling of biochar for Cr(VI) reduction, *J. Hazard. Mater.*, 2019, **378**, 120705.

39 X. Xiao and B. Chen, A direct observation of the fine aromatic clusters and molecular structures of biochars, *Environ. Sci. Technol.*, 2017, **51**, 5473–5482.

40 S. Y. Chen, A. Gloter, A. Zobelli, L. Wang, C. H. Chen and C. Colliex, Electron energy loss spectroscopy and ab initio investigation of iron oxide nanomaterials grown by a hydrothermal process, *Phys. Rev. B: Condens. Matter Mater. Phys.*, 2009, **79**, 104103.

41 X. Xu, X. Cao, L. Zhao, H. Wang, H. Yu and B. Gao, Removal of Cu, Zn, and Cd from aqueous solutions by the dairy manure-derived biochar, *Environ. Sci. Pollut. Res.*, 2013, **20**, 358–368.

42 A. R. Betts, N. Chen, J. G. Hamilton and D. Peak, Rates and mechanisms of Zn^{2+} adsorption on a meat and bonemeal biochar, *Environ. Sci. Technol.*, 2013, **47**, 14350–14357.

43 Y. Yao, B. Gao, J. Chen and L. Yang, Engineered biochar reclaiming phosphate from aqueous solutions: mechanisms and potential application as a slow-release fertilizer, *Environ. Sci. Technol.*, 2013, **47**, 8700–8708.

44 T. Sun, B. D. Levin, J. J. Guzman, A. Enders, D. A. Muller, L. T. Angenent and J. Lehmann, Rapid electron transfer by the carbon matrix in natural pyrogenic carbon, *Nat. Commun.*, 2017, **8**, 14873.

45 B. Pan, H. Li, D. Lang and B. S. Xing, Environmentally persistent free radicals: Occurrence, formation mechanisms and implications, *Environ. Pollut.*, 2019, **248**, 320–331.

46 W. Xu, J. J. Pignatello and W. A. Mitch, Role of black carbon electrical conductivity in mediating hexahydro-1,3,5-trinitro-1,3,5-triazine (RDX) transformation on carbon surfaces by sulfides, *Environ. Sci. Technol.*, 2013, **47**, 7129–7136.

47 S. Liao, B. Pan, H. Li, D. Zhang and B. S. Xing, Detecting free radicals in biochars and determining their ability to inhibit the germination and growth of corn, wheat and rice seedlings, *Environ. Sci. Technol.*, 2014, **48**, 8581–8587.